Struct Multidisc Optim
DOI 10.1007/s00158-017-1760-y

RESEARCH PAPER

Local maximum-entropy based surrogate model and its application to structural reliability analysis

Jiang Fan[1,2,3] · Huming Liao[1] · Hao Wang[4] · Junheng Hu[1] · Zhiying Chen[1] · Jian Lu[5] · Bo Li[4]

Received: 4 January 2017 / Revised: 29 June 2017 / Accepted: 3 July 2017

Abstract A novel surrogate model based on the Local Maximum-Entropy (LME) approximation is proposed in this paper. By varying the degrees of locality, the LME-based surrogate model is constructed according to the local behavior of the response function at the prediction points. The proposed method combines the advantages of both local and global approximation schemes. The robustness and effectiveness of the model are systematically investigated by comparing with the conventional surrogate models (such as Polynomial regression, Radial basis function, and Kriging model) in three types of test problems. In addition, the performance of the LME-based surrogate model is evaluated by an industry case of turbine disk reliability analysis (TDRA) involving random geometric parameters. In TDRA, two LME-based surrogate models are built including a 1^{st} surrogate model employed in the sensitivity analysis to determine the key random variables and a 2^{nd} surrogate model utilized in Monte-Carlo Simulations (MCS) to predict the Low Cycle Fatigue (LCF) life of turbine disks. Finally, a model-based Uncertainty Quantification (UQ) analysis is performed to rigorously quantify the uncertainties of the physical system and fidelity of surrogate model predictions simultaneously. Results show that the LME-based surrogate model can achieve a desirable level of accuracy and robustness with reduced number of sample points, which indicates the proposed method possess the potential for approximating highly nonlinear limit state functions and applicable for structural reliability analysis.

Keywords Local Maximum-Entropy · Surrogate model · Structural reliability analysis · Turbine disk · Uncertainty quantification

✉ Jian Lu
luj@giaaet.com

✉ Bo Li
bxl295@case.edu

[1] School of Energy and Power Engineering, Beihang University, Beijing 100191, China

[2] Beijing Key Laboratory of Aero-Engine Structure and Strength, Beijing 100191, China

[3] Collaborative Innovation Center of Advanced Aero-Engine, Beijing 100191, China

[4] Department of Mechanical and Aerospace Engineering, Case Western Reserve University, Cleveland, OH 44106, USA

[5] Guangdong Institute of Aeronautics and Astronautics Equipment & Technology, Zhuhai, Guangdong 519000, China

1 Introduction

The structural reliability analysis deals with the statistical nature of structural safety analysis and design with many random variables. Monte-Carlo Simulations (MC) have been widely used to estimate the failure probability of structural systems. The MCS requires hundreds and thousands of evaluations of the performance function of a complex structural system. Such calculations can be performed efficiently when the performance function $y(\boldsymbol{x})$ is expressed as an explicit form or simple analytical form in terms of the random variables $\boldsymbol{x}$. When the performance functions are implicit, however, such calculations require additional effort and will be time-consuming. For instance, such implicit performance functions normally occur when costly physical experiments or computationally intensive numerical analyses, such as 3-D finite element simulations,

Published online: 28 July 2017

must be adopted for the mechanical analysis of a structural system (cf. Deng 2006). The enormous computational cost of running complex and high fidelity simulations makes it impractical. A preferable strategy is to replace the expensive simulation models by surrogate models, also often referred to as metamodels or response surface models, during the reliability analysis process (cf. Jin et al. 2001).

Surrogate models have been widely employed for structural reliability analysis. The classic Polynomial Regression (PR) is the original and commonly used form for surrogate models in structural reliability analysis. Wong (1985) first proposed a complete, quadratic form polynomial and applied it to reliability analysis, in which the number of polynomials and the required sampling points increase rapidly with the number of random variables. Thereafter, many studies (see, e.g. Bucher and Bourgund 1990; Rajashekhar and Ellingwood 1993; Liu and Moses 1994; Kim and Na 1997; Das and Zheng 2000; Guan and Melchers 2001; Kaymaz and McMahon 2005; Nguyen et al. 2009) have been made to improve the performance of the PR-based surrogate models. Nevertheless, the performance of the PR model is limited in applications with highly nonlinear functions as noted in Barton (1992). Higher-order polynomials can be adopted to overcome this difficulty, but instabilities may arise. In addition, it may be challenging to provide sufficient sampling data for the evaluation of the coefficients in high-order polynomial functions, particularly for high-dimensional problems.

In this context, alternative surrogate modeling methods were introduced to address the challenges in PR-based surrogate models for structural reliability analysis. Papadrakakis et al. (1996), Hurtado and Alvarez (2001), and Elhewy et al. (2006) used Neural Networks to reliability analysis in conjunction with MCS. Deng (2006) proposed three Radial Basis Function (RBF) network methods to compute the performance function derivatives and then to combine them with the conventional MCS, First-Order Reliability Methods (FORM) and the Second Order Reliability Methods (SORM). Most (2007) presented an efficient adaptive response surface approach, where Support Vector Machines (SVM) were used to classify the failure and safe domain. Guo and Bai (2009) proposed a least squares SVM for regression into reliability analysis and the results demonstrate excellent accuracy and reduced computational cost than the SVM-based reliability method. Song et al. (2013) proposed a Virtual Support Vector Machine (VSVM). In this method, virtual samples are generated near the limit state function and the exact function values are adopted for approximations of virtual samples to improve the accuracy of the resulting VSVM decision function. Panda and Manohar (2008) proposed the Kriging (KG) method and compared it with the commonly used surrogate models. Echard et al. (2011) presented a KG enhanced MCS method in reliability analysis with improved accuracy and efficiency. Youn and Choi (2004) and Song et al. (2011) have applied the Moving Least Squares (MLS) method to reliability based design optimization, which performs well in uncertainty design. Li et al. (2012) proposed a doubly weighted MLS and applied it to structural reliability analysis.

Among the aforementioned surrogate models, the RBF model is a global approximation scheme, in which the shape function covers the whole range of the domain. Approximation of the response function at a given point by the RBF surrogate model requires all the sample data in the design space. On the contrary, KG model is a local approximation scheme and can require significant computational time if the sample data set is large, due to the expensive inner parameter optimization. Moreover, in the original KG model, the correlation matrix becomes singular if multiple sample points are spaced closely to each other or if the sample points are generated from particular designs as noted in Jin et al. (2001). To fit the true response function more accurately, Zhao et al. (2011) proposed a dynamic KG method. Zhao et al. (2013) constructed a conservative surrogate model using weighted KG variance, which reduces fluctuation in the KG prediction bound and performs better than the constant safety margin approach.

In this paper, we propose a novel surrogate model based on Local Maximum-Entropy (LME) approximation to combine the advantages of both the local and global approximation schemes. LME approximation is originally introduced by Arroyo and Ortiz (2006) for data interpolation. It has been widely used to obtain approximations in meshfree methods (see, e.g. Li et al. 2010; Ortiz et al. 2010; González et al. 2010; Fraternali et al. 2012; Wu et al. 2013; Ullah et al. 2013; Rosolen and Arroyo 2013; Kochmann and Venturini 2014). The LME shape functions are calculated by minimizing an objective function which integrates the Jaynes' principle of maximum entropy (Max-Ent) and Delaunay triangulation in the sense of Pareto optimality. The global Max-Ent approximation assures unbiased statistical inference based on the sample data over the entire domain. Meanwhile, the Delaunay triangulation defines the most local shape functions of least width. The width of LME shape functions is allowed to depend on the location of the prediction point. In order to achieve optimal degrees of locality, but maintain least unbiased contributions from the set of sample points, the LME shape functions can be adjusted according to the local behavior of the response function by varying a dimensionless parameter γ. The LME-based method enables the construction of surrogate models of a high level of accuracy with a significant reduction of the number of sample points. Nevertheless, the original LME approximation scheme only satisfies a weak Kronecker-delta property. Therefore, the function values at

the sample points predicted by the surrogate model are not equivalent to the exact solutions except the one at the vertices of the convex hull of the sample points. In order to overcome this deficiency, in this work, a group of optimized coefficients $\boldsymbol{C}$ is introduced to replace the actual values of the response function at sample points within an optimal local neighborhood. By this means, the LME-based surrogate model is enforced to reproduce the exact values of the response function at all the sample points in the local neighborhood of the prediction point. The performance of the proposed surrogate model is systematically investigated by comparing to the conventional surrogate models (PR, RBF, and KG) in three types of engineering problems. The robustness and efficiency of the LME-based surrogate model are further demonstrated in the application of a turbine disk reliability analysis with uncertainties in the geometric parameters. Finally a model-based Uncertainty Quantification (UQ) analysis is performed to rigorously quantify the uncertainties of the physical system and fidelity of surrogate model predictions simultaneously. The results show that LME-based surrogate model excels in high-order nonlinearity problems. In addition, the calculation of the LME shape functions requires fewer sampling points and can be carried out robustly and efficiently in any spatial dimensions. The derivatives of the LME shape functions are auxiliary outputs of the computation without any additional computational cost, which increases the transparency of the model.

The remainder of this paper is organized as follows. Section 2 introduces the various surrogate model constructing methods. Section 3 investigates the performance of the LME-based surrogate model by comparing with PR, RBF and KG surrogate models in three types of engineering test problems. Results from applying the proposed surrogate model to an industry application are presented in Section 4. Some concluding remarks are finally collected in Section 5.

2 Surrogate models

For the sake of completeness of the paper, we briefly summarize the various conventional methods for the construction of surrogate models, including Polynomial Regression (PR), Radial Basis Functions (RBF) and Kriging model (KG).

2.1 Polynomial regression (PR)

PR (see Queipo et al. 2005) assumes the following relation between the predicted function $\hat{y}$ and K polynomial basis functions p_j at a given prediction point $\boldsymbol{x}$:

$$\hat{y}(\boldsymbol{x}) = \sum_{j=1}^{K} \beta_j p_j(\boldsymbol{x}). \tag{1}$$

The coefficients $\boldsymbol{\beta} = [\beta_1\ \beta_2\ \dots\ \beta_K]^T$ can be obtained by enforcing the following conditions at N samples $y(\boldsymbol{x}^{(i)}), i = 1, \dots, N$:

$$y(\boldsymbol{x}^{(i)}) = \sum_{j=1}^{K} \beta_j p_j(\boldsymbol{x}^{(i)}), \tag{2}$$

where $\boldsymbol{x}^{(i)}$ is a n dimensional vector $\boldsymbol{x}^{(i)} = \left[x_1^{(i)}\ x_2^{(i)}\ \dots\ x_n^{(i)}\right]^T$, and these equations can be represented in matrix form:

$$\boldsymbol{y} = \boldsymbol{X}\boldsymbol{\beta}, \tag{3}$$

where $\boldsymbol{y} = [y(\boldsymbol{x}^{(1)})\ y(\boldsymbol{x}^{(2)})\ \dots\ y(\boldsymbol{x}^{(N)})]^T$, $\boldsymbol{X}$ is a $N \times K$ matrix containing the basis functions evaluated at the sample points. The number of sample points N should be consistent with the number of basis functions considered K (typically $N \geq K$). If the sample points and basis function are taken arbitrarily, some columns of X can be linearly dependent. If $N \geq K$ and $\text{rank}(\boldsymbol{X}) = K$, a solution of (3) in the least-squares sense can be computed through $\boldsymbol{X}^+$, the pseudoinverse (or generalized inverse) of $\boldsymbol{X}$ (see Golub and Van Loan 2012):

$$\boldsymbol{\beta} = \boldsymbol{X}^+ = (\boldsymbol{X}^T\boldsymbol{X})^{-1}\boldsymbol{X}^T\boldsymbol{y}. \tag{4}$$

Estimating K is not so simple. The polynomial approximation (1) of order K of an underlying function $y(\boldsymbol{x})$ is similar in some ways to a Taylor series expansion of $y(\boldsymbol{x})$ truncated after $K + 1$ terms, which means the polynomial approximation is a type of local approximation. This suggests that greater values of K (i.e. more Taylor expansion terms) will usually yield a more accurate approximation. However, the greater the number of terms, the more flexible the model becomes and we come up against the danger of overfitting any noise that may be corrupting the underlying response. Also, we run the risk of building an excessively *snaking* polynomial with poor generalization (cf. Forrester and Keane 2009). The simplest examples of regression models are the first- and second-order polynomial models. A second-order polynomial surrogate model with second-order polynomial cross terms can be expressed as:

$$\hat{y}(\boldsymbol{x}) = \hat{y}([x_1\ x_2\ \dots\ x_n]^T) = \alpha_0 + \sum_{j=1}^{n} \alpha_j x_j + \sum_{i=1}^{n}\sum_{j\leq i}^{n} \alpha_{ij} x_i x_j. \tag{5}$$

When dealing with large-scale problems or high-order nonlinearity problems, the unknown parameters of a PR model increases sharply, which may cause instability or require a large number of samples. In this paper, a second-order PR model (PR2) and a fourth-order PR model (PR4) with cross terms are selected as the surrogate models to compare with the LME-based surrogate model.

2.2 Radial basis functions (RBF)

RBF approximation (see Forrester and Keane 2009; Wild et al. 2008) predicts the value of the function at a given point $\boldsymbol{x}$ by the linear combinations of K radially symmetric functions ϕ:

$$\hat{y}(\boldsymbol{x}) = \sum_{j=1}^{K} \lambda_j \phi(\| \boldsymbol{x} - \boldsymbol{c}^{(j)} \|), \tag{6}$$

where $\boldsymbol{\lambda} = [\lambda_1 \ \lambda_2 \ \ldots \ \lambda_K]^T$ is the vector of model parameters, and $\boldsymbol{c}^{(j)}$, $j = 1, \ldots, K$, are the centers of the basis functions.

Similar to polynomial regression, the model parameters $\boldsymbol{\lambda}$ can be computed by:

$$\boldsymbol{\lambda} = \boldsymbol{\Phi}^{+} = (\boldsymbol{\Phi}^T \boldsymbol{\Phi})^{-1} \boldsymbol{\Phi}^T \boldsymbol{y}, \tag{7}$$

where again $\boldsymbol{y} = [y(\boldsymbol{x}^{(1)}) \ y(\boldsymbol{x}^{(2)}) \ \ldots \ y(\boldsymbol{x}^{(N)})]^T$, and $N \times K$ matrix $\boldsymbol{\Phi}$ is defined as:

$$\boldsymbol{\Phi} = \begin{bmatrix} \phi(\| \boldsymbol{x}^{(1)} - \boldsymbol{c}^{(1)} \|) & \phi(\| \boldsymbol{x}^{(1)} - \boldsymbol{c}^{(2)} \|) & \cdots & \phi(\| \boldsymbol{x}^{(1)} - \boldsymbol{c}^{(K)} \|) \\ \phi(\| \boldsymbol{x}^{(2)} - \boldsymbol{c}^{(1)} \|) & \phi(\| \boldsymbol{x}^{(2)} - \boldsymbol{c}^{(2)} \|) & \cdots & \phi(\| \boldsymbol{x}^{(2)} - \boldsymbol{c}^{(K)} \|) \\ \vdots & \vdots & \ddots & \vdots \\ \phi(\| \boldsymbol{x}^{(N)} - \boldsymbol{c}^{(1)} \|) & \phi(\| \boldsymbol{x}^{(N)} - \boldsymbol{c}^{(2)} \|) & \cdots & \phi(\| \boldsymbol{x}^{(N)} - \boldsymbol{c}^{(K)} \|) \end{bmatrix}. \tag{8}$$

If selecting $N = K$ (i.e. the number of basis functions equals to the number of samples), and if $\boldsymbol{x}^{(j)} = \boldsymbol{c}^{(j)}$ (i.e. the centers of the basis functions coincide with the data points), $\boldsymbol{\Phi}$ is a regular square matrix (and thus, $\boldsymbol{\lambda} = \boldsymbol{\Phi}^{-1} \boldsymbol{y}$). Typical choices for the basis functions are

$$\phi(r) = \begin{cases} r & \text{, linear} \\ r^3 & \text{, cubic} \\ r^2 \ln r & \text{, thin plate spline} \end{cases}, \tag{9}$$

more flexibility can be obtained by using parametric basis functions such as

$$\phi(r) = \begin{cases} \exp(-r^2/2\sigma^2) & \text{, Gaussian} \\ (r^2 + \sigma^2)^{1/2} & \text{, multiquadric} \\ (r^2 + \sigma^2)^{-1/2} & \text{, inverse multi-quadric} \end{cases}. \tag{10}$$

In this paper, an RBF surrogate model with Gaussian basis function, which is a type of global approximation and its shape function covers the whole range of the domain, is selected to compare with the LME-based surrogate model.

2.3 Kriging model (KG)

KG (see Journel and Huijbregts 1978; Simpson et al. 2001) postulates a combination of a global model plus departures:

$$y(\boldsymbol{x}) = \boldsymbol{g}(\boldsymbol{x})^T \boldsymbol{\beta} + Z(\boldsymbol{x}), \tag{11}$$

where $y(\boldsymbol{x})$ is the unknown function of interest, $\boldsymbol{g}(\boldsymbol{x}) = [g_1(\boldsymbol{x}) \ g_2(\boldsymbol{x}) \ \ldots \ g_K(\boldsymbol{x})]^T$ are known (usually polynomial) functions of $\boldsymbol{x}$, $\boldsymbol{\beta} = [\beta_1 \ \beta_2 \ \ldots \ \beta_K]^T$ are the unknown model parameters, and $Z(\boldsymbol{x})$ is assumed to be a realization of a stochastic process with mean zero, variance σ^2 and non-zero covariance.

The regression part $\boldsymbol{g}(\boldsymbol{x})^T \boldsymbol{\beta}$ approximates globally the function $y(\boldsymbol{x})$, and $Z(\boldsymbol{x})$ takes into account localized variations. The covariance matrix of $Z(\boldsymbol{x})$ is given as:

$$Cov[Z(\boldsymbol{x}^{(i)}) Z(\boldsymbol{x}^{(j)})] = \sigma^2 \boldsymbol{R}([R(\boldsymbol{x}^{(i)}, \boldsymbol{x}^{(j)})]), \tag{12}$$

where $\boldsymbol{R}$ is a $N \times N$ correlation matrix with $R_{ij} = R(\boldsymbol{x}^{(i)}, \boldsymbol{x}^{(j)})$. Here $R(\boldsymbol{x}^{(i)}, \boldsymbol{x}^{(j)})$ is the correlation function between sampled data points $\boldsymbol{x}^{(i)}$ and $\boldsymbol{x}^{(j)}$.

Thus, the KG surrogate model is defined as:

$$\hat{y}(\boldsymbol{x}) = \boldsymbol{g}(\boldsymbol{x})^T \boldsymbol{\beta} + \boldsymbol{r}^T(\boldsymbol{x}) \boldsymbol{R}^{-1} (\boldsymbol{y} - \boldsymbol{G}\boldsymbol{\beta}), \tag{13}$$

where $\boldsymbol{r}(\boldsymbol{x}) = [R(\boldsymbol{x}, \boldsymbol{x}^{(1)}) \ \ldots R(\boldsymbol{x}, \boldsymbol{x}^{(N)})]^T$, $\boldsymbol{y} = [y(\boldsymbol{x}^{(1)}) \ y(\boldsymbol{x}^{(2)}) \ \ldots \ y(\boldsymbol{x}^{(N)})]^T$, and $\boldsymbol{G}$ is a $N \times K$ matrix with $G_{ij} = g_j(\boldsymbol{x}^{(i)})$.

A variety of functions can be chosen as the correlation function $\boldsymbol{R}$, such as

$$R(\boldsymbol{x}^{(i)}, \boldsymbol{x}^{(j)}) = \begin{cases} \prod_{k=1}^{n} \exp(-\theta_k |d_k|^2) & \text{, Gaussian} \\ \prod_{k=1}^{n} \exp(-\theta_k |d_k|) & \text{, Exponential} \\ \prod_{k=1}^{n} [(1 + \theta_k |d_k|) \exp(-\theta_k |d_k|)] & \text{, Matern linear} \\ \prod_{k=1}^{n} [(1 + \theta_k |d_k| + \theta_k^2/3) \exp(-\theta_k |d_k|)] & \text{, Matern cubic} \end{cases}, \tag{14}$$

where θ_k is the unknown vector of correlation parameters used to be fitted this KG model, and d_k is the distance between any two sample points $\boldsymbol{x}^{(i)}$ and $\boldsymbol{x}^{(j)}$ of the k^{th} components. In the following paper, a KG surrogate model with Gaussian correlation function (referred to KG1) and a KG surrogate model with Exponential correlation function (referred to KG2) are selected to compare with LME-based surrogate model.

2.4 Surrogate model based on the local maximum entropy (LME) approximation scheme

In this paper, we introduce a novel surrogate modeling method based on the LME approximation scheme. We consider an implicit performance function $y(\boldsymbol{x})$ where $\boldsymbol{x} = [x_1\ x_2\ \ldots\ x_n]^T$ is an n dimensional random variable. In the LME method, the implicit performance function at a given prediction point $\boldsymbol{x}$ is approximated by:

$$\hat{y}(\boldsymbol{x}) = \sum_{i=1}^{N} y(\boldsymbol{x}^{(i)}) p_i(\boldsymbol{x}), \tag{15}$$

where $\boldsymbol{x}^{(i)} \in \boldsymbol{X}$, $\boldsymbol{X} = \{\boldsymbol{x}^{(i)}, i = 1, 2, ..., N\}$ is the set of N sample points and $y(\boldsymbol{x}^{(i)})$ is the value of the corresponding response function at $\boldsymbol{x}^{(i)}$, respectively. The sample points and response data are usually obtained via physical experiments or numerical analysis, such as finite element simulations for a complicated structural system. $p_i(\boldsymbol{x})$ is the LME shape function of the sample point $\boldsymbol{x}^{(i)}$ at a given prediction point $\boldsymbol{x}$.

In this section, we present how to build the LME shape functions as introduced by Arroyo and Ortiz (2006). Let $\Omega_{Max-Ent}$ be the convex hull of the sample point set $\boldsymbol{X}$, and the shape function of the sample point $\boldsymbol{x}^{(i)}$ at a given prediction point $\boldsymbol{x}$ is defined as the solution of problem (16):

$$\begin{aligned}
(\text{Max-Ent})_\beta \text{Minimize}\, f_\beta(\boldsymbol{x}, \boldsymbol{p}) \equiv\ & \beta \sum_{i=1}^{N} p_i |\boldsymbol{x} - \boldsymbol{x}^{(i)}|^2 \\
& + \sum_{i=1}^{N} p_i \log p_i, \\
\text{given } \forall \boldsymbol{x} \in \Omega_{Max-Ent} \quad & p_i(\boldsymbol{x}) \geqslant 0,\ i \in [1, N], \\
& \sum p_i(\boldsymbol{x}) = 1, \\
& \sum p_i(\boldsymbol{x}) \boldsymbol{x}^{(i)} = \boldsymbol{x},
\end{aligned} \tag{16}$$

where $\beta \in \mathbb{R}^+$ is a Pareto optimal parameter used to ponder the locality term against the entropy term in the objective function.

The constraints in the minimization problem ensure that the resulting shape functions satisfy the zeroth and first order consistency. Consequently, the LME-based surrogate model is able to exactly reproduce constant and linear functions. The solution of the minimization problem is unique and therefore, the LME shape functions can be directly calculated as:

$$p_i(\boldsymbol{x}) = \frac{1}{Z(\boldsymbol{x}, \boldsymbol{\lambda}^*(\boldsymbol{x}))} \exp[-\beta |\boldsymbol{x} - \boldsymbol{x}^{(i)}|^2 + \boldsymbol{\lambda}^*(\boldsymbol{x}) \cdot (\boldsymbol{x} - \boldsymbol{x}^{(i)})], \tag{17}$$

where:

$$\boldsymbol{\lambda}^*(\boldsymbol{x}) = \arg \min_{\boldsymbol{\lambda} \in \mathbb{R}^n} \log Z(\boldsymbol{x}, \boldsymbol{\lambda}), \tag{18}$$

$$Z(\boldsymbol{x}, \boldsymbol{\lambda}) = \sum_{i=1}^{N} \exp[-\beta |\boldsymbol{x} - \boldsymbol{x}^{(i)}|^2 + \boldsymbol{\lambda} \cdot (\boldsymbol{x} - \boldsymbol{x}^{(i)})]. \tag{19}$$

The parameter β determines the support width of the shape functions and is allowed to depend on the position of the sample points. This dependence can be adjusted in order to achieve varying degrees of locality, which gives us the great advantage for the construction of anisotropic shape functions and high-order approximations.

In practice, a dimensionless parameter γ is used to control the locality of the LME shape functions, which is related to β by:

$$\gamma = \beta h^2, \tag{20}$$

where h is a local characteristic length of the prediction point $\boldsymbol{x}$. As Fig. 1 shown, γ usually ranges from 0.1 to 6.8 and determines the locality of the LME shape functions, which introduces a seamless bridge between local approximation and global approximation. The characteristic length of a given prediction point $\boldsymbol{x}$ is calculated by finding the sample points $\boldsymbol{x}^{(i)}$ in the neighborhood of $\boldsymbol{x}$, and then finding the nearest sample point $\boldsymbol{x}^{(j)}$ to $\boldsymbol{x}^{(i)}$. Thus, the Euclidean distance between $\boldsymbol{x}^{(i)}$ and $\boldsymbol{x}^{(j)}$ is defined as h of $\boldsymbol{x}$ as shown in Fig. 1. It is worthy mentioning that, due to the locality of the LME shape functions, only the nearest neighbors $\boldsymbol{X}_{\text{local}} \equiv \{\boldsymbol{x}^{(i)}, i = 1, 2, ..., M, M \leqslant N\}$ of the prediction point $\boldsymbol{x}$ contributes the most to approximate the value of the response function at $\boldsymbol{x}$. A trunction error can be introduced to select the sample points whose shape function value larger than an user defined tolerance p_{tol} (e.g., in our implementation $p_{tol} = 1.0 \times 10^{-5}$). Consequently, the construction of the surrogate model based on LME approximation is highly localized and the number of sample points needed for the prediction of $\hat{y}(\boldsymbol{x})$ can be greatly reduced.

Finally, the calculation of the shape function in (17) requires to find $\boldsymbol{\lambda}^*(\boldsymbol{x})$, the minimizer of the objective function $\log Z(\boldsymbol{x}, \boldsymbol{\lambda}^*(\boldsymbol{x}))$. This unconstrained minimization problem with convexing can be solved efficiently and robustly by a combination of Newton-Raphson algorithm and Nelder-Mead simplex algorithm (see Nelder and Mead 1965).

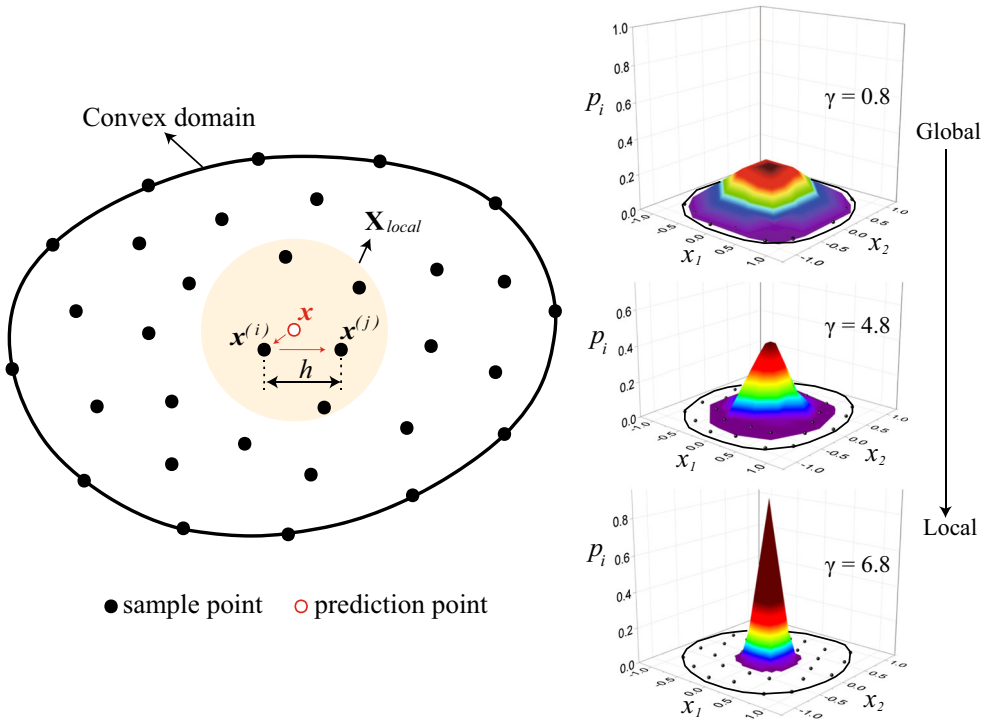

Fig. 1 The shape functions with different γ and the definition of local characteristic length h in a two-dimensional convex domain

Nevertheless, the LME shape function only satisfies a weak Kronecker-delta property, which means the approximated function value equals to the exact value only at the vertices of the convex hull of the set of sample points. As a consequence, the predicted function value at an interior sample point $\boldsymbol{x}^{(j)}$ by the LME-based surrogate model does not equal to the exact value, i.e.

$$\hat{y}(\boldsymbol{x}^{(j)}) = \sum_{i=1}^{M} y(\boldsymbol{x}^{(i)}) p_i(\boldsymbol{x}^{(j)}) \neq y(\boldsymbol{x}^{(j)}), \text{ for } \forall \boldsymbol{x}^{(j)} \notin \mathcal{A}, \tag{21}$$

where $\mathcal{A}$ is the set of vertices of $\Omega_{Max-Ent}$. To enforce this equivalence relationship and improve the accuracy of LME-based surrogate model, in our implementation, $y(\boldsymbol{x}^{(i)})$ is replaced by an optimized coefficient C_i, such that,

$$\hat{y}(\boldsymbol{x}) = \sum_{i=1}^{M} C_i p_i(\boldsymbol{x}) = y(\boldsymbol{x}), \text{ for } \forall \boldsymbol{x} \in \{\boldsymbol{x}^{(i)}, \boldsymbol{x}^{(i)} \in \boldsymbol{X}_{\text{local}}\}, \tag{22}$$

Under this constraint, the surrogate model is enforced to reproduce the exact response function values at all the sample points in the local neighbourhood of $\boldsymbol{x}$ as Fig. 2 shown. To determine the optimized coefficients C_i, given function values at the sample points, the shape functions $p_i(\boldsymbol{x})$ needs to be calculated at for $\forall \boldsymbol{x} \in \{\boldsymbol{x}^{(i)}, \boldsymbol{x}^{(i)} \in \boldsymbol{X}_{\text{local}}\}$ as (22) indicates. Since the characteristic length h of the prediction point $\boldsymbol{x}$ is a constant, the support-width of the shape function $p_i(\boldsymbol{x})$ is determined by the given γ. Thus, for $\forall \boldsymbol{x} \in \{\boldsymbol{x}^{(i)}, \boldsymbol{x}^{(i)} \in \boldsymbol{X}_{\text{local}}\}$, we obtain a system of linear equations, i.e.,

$$\begin{aligned}
\hat{y}(\boldsymbol{x}^{(1)}) &= C_1 p_1(\boldsymbol{x}^{(1)}) + C_2 p_2(\boldsymbol{x}^{(1)}) + \ldots \\
&\quad + C_M p_M(\boldsymbol{x}^{(1)}) = y(\boldsymbol{x}^{(1)}) \\
\hat{y}(\boldsymbol{x}^{(2)}) &= C_1 p_1(\boldsymbol{x}^{(2)}) + C_2 p_2(\boldsymbol{x}^{(2)}) + \ldots \\
&\quad + C_M p_M(\boldsymbol{x}^{(2)}) = y(\boldsymbol{x}^{(2)}) \\
&\vdots \\
\hat{y}(\boldsymbol{x}^{(M)}) &= C_1 p_1(\boldsymbol{x}^{(M)}) + C_2 p_2(\boldsymbol{x}^{(M)}) + \ldots \\
&\quad + C_M p_M(\boldsymbol{x}^{(M)}) = y(\boldsymbol{x}^{(M)})
\end{aligned}, \tag{23}$$

Rewriting (23) in the matrix form gives,

$$\underbrace{\begin{pmatrix} p_1(\boldsymbol{x}^{(1)}) & p_2(\boldsymbol{x}^{(1)}) & \ldots & p_M(\boldsymbol{x}^{(1)}) \\ p_1(\boldsymbol{x}^{(2)}) & p_2(\boldsymbol{x}^{(2)}) & \ldots & p_M(\boldsymbol{x}^{(2)}) \\ \vdots & \vdots & \ddots & \vdots \\ p_1(\boldsymbol{x}^{(M)}) & p_2(\boldsymbol{x}^{(M)}) & \ldots & p_M(\boldsymbol{x}^{(M)}) \end{pmatrix}}_{\boldsymbol{p}} \underbrace{\begin{pmatrix} C_1 \\ C_2 \\ \vdots \\ C_M \end{pmatrix}}_{\boldsymbol{C}} = \underbrace{\begin{pmatrix} y(\boldsymbol{x}^{(1)}) \\ y(\boldsymbol{x}^{(2)}) \\ \vdots \\ y(\boldsymbol{x}^{(M)}) \end{pmatrix}}_{\boldsymbol{y}}, \tag{24}$$

where $\boldsymbol{p}$ is a $M \times M$ square matrix, and M is the number of sample points in the neighborhood of the prediction point and determined by the locality of the shape functions (e.g., Fig. 2 shows a 6×6 square matrix for $\boldsymbol{x}_a$ and 4×4 square matrix for $\boldsymbol{x}_b$). Finally (24) can be abbreviated as:

$$\boldsymbol{pC} = \boldsymbol{y}, \tag{25}$$

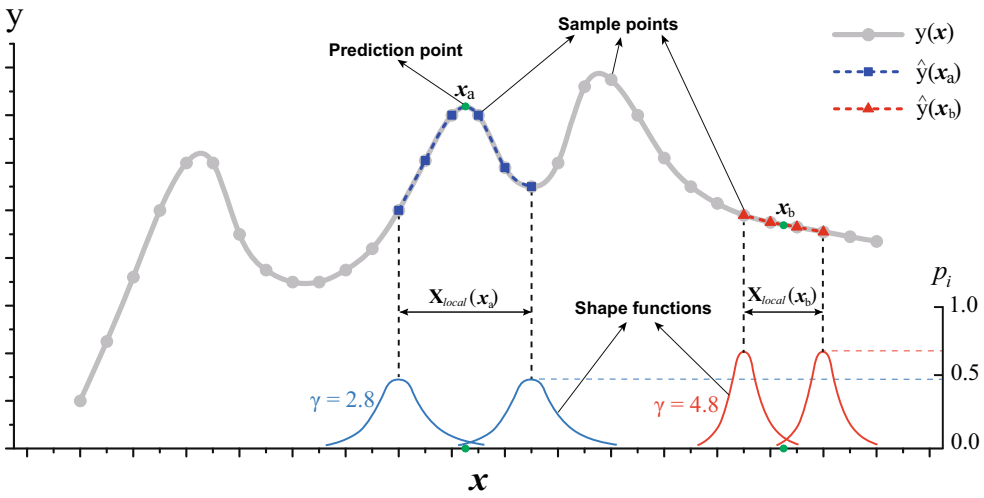

Fig. 2 $\boldsymbol{X}_{local}(\boldsymbol{x}_a)$ is the local neighbourhood of prediction point $\boldsymbol{x}_a$ with $\gamma = 2.8$ (*blue curves* are the shape functions with $\gamma = 2.8$) in a one-dimensional case, while predicting $\hat{y}(\boldsymbol{x}_a)$ the surrogate model will get through all the sample points in $\boldsymbol{X}_{local}(\boldsymbol{x}_a)$. $\boldsymbol{X}_{local}(\boldsymbol{x}_b)$ is the local neighbourhood of prediction point $\boldsymbol{x}_b$ with $\gamma = 4.8$ (*red curves* are the shape functions with $\gamma = 4.8$), while predicting $\hat{y}(\boldsymbol{x}_b)$, the surrogate model will get through all the sample points in $\boldsymbol{X}_{local}(\boldsymbol{x}_b)$

thus the optimized coefficients $\boldsymbol{C}$ can be calculated by,

$$\boldsymbol{C} = \boldsymbol{p}^{-1}\boldsymbol{y}. \tag{26}$$

Note that, in the RBF method, a similar optimization scheme is utilized to obtain the model parameters $\boldsymbol{\lambda}$ (Section 2.2). However, there is no explicit guideline to determine the size of the $N \times K$ matrix $\boldsymbol{\Phi}$ as (8) defined. If selecting $N = K$, then $\boldsymbol{\Phi}$ is a $N \times N$ square matrix involving all the sample points in the global domain, which results in a time-consuming computation of the inverse matrix $\boldsymbol{\Phi}^{-1}$, especially for high-dimensional nonlinear problems. In contrast, the calculation of the coefficients $\boldsymbol{C}$ in the LME-based surrogate model only requires the inversion of a $M \times M$ square matrix, and usually $M << N$. In addition, the number of sample points in the neighborhood of a prediction point can be set by the user according to the nonlinearity of the response function and adjusted by varying the parameter γ. Furthermore, different γ can be adopted when evaluating the function values at different prediction points, which allows the user to adaptively control the number of sample points at the design subspaces and reduce the number of experiments or complex numerical tests. As a result of the competition between Jaynes' principle of maximum entropy and Delaunay triangulation in the LME approximation scheme, the construction of the LME-based surrogate model always requires the local information but assures unbiased statistical inference in a global sense.

Under this condition, the implicit performance function at a given prediction point $\boldsymbol{x}$ is approximated by:

$$\hat{y}(\boldsymbol{x}) = \sum_{i=1}^{M} C_i\, p_i(\boldsymbol{x}). \tag{27}$$

and the algorithm resulting from the preceding scheme is listed in Table 1.

Meanwhile, derivatives of the LME shape functions will be the auxiliary outputs of the computation, which are defined as:

$$\nabla p_i(\boldsymbol{x}) = -p_i(\boldsymbol{x})\boldsymbol{J}(\boldsymbol{x}, \boldsymbol{\lambda}^*(\boldsymbol{x}))^{-1}(\boldsymbol{x} - \boldsymbol{x}^{(i)}), \tag{28}$$

where:

$$\boldsymbol{J}(\boldsymbol{x}, \boldsymbol{\lambda}^*(\boldsymbol{x})) = \sum_{i=1}^{N} p_i(\boldsymbol{x}, \boldsymbol{\lambda})(\boldsymbol{x} - \boldsymbol{x}^{(i)}) \otimes (\boldsymbol{x} - \boldsymbol{x}^{(i)}) - \boldsymbol{r}(\boldsymbol{x}, \boldsymbol{\lambda}) \otimes \boldsymbol{r}(\boldsymbol{x}, \boldsymbol{\lambda}), \tag{29}$$

and

$$\boldsymbol{r}(\boldsymbol{x}, \boldsymbol{\lambda}) \equiv \partial_{\boldsymbol{\lambda}} \log \boldsymbol{Z}(\boldsymbol{x}, \boldsymbol{\lambda}) = \sum_{i=1}^{N} p_i(\boldsymbol{x}, \boldsymbol{\lambda})(\boldsymbol{x} - \boldsymbol{x}^{(i)}). \tag{30}$$

3 Performance of surrogate models

3.1 Test problems

To systematically investigate the performance of the LME-based surrogate model and compare it with the conventional surrogate models (PR2, PR4, RBF, KG1 and KG2) as described foregoing, three explicit mathematical functions are selected as test cases. These functions are classified based on the following representative features of engineering design problems as introduced by Jin et al. (2001).

Problem scale Two relative scales are considered, small scale and large scale. In this paper, small scale is defined with the number of variables ≤ 3, while the large scale is defined with the number of variables ≥ 4.

Table 1 The LME-based surrogate model modeling algorithm

Algorithm	Calculate $\hat{y}(\boldsymbol{x})$ for prediction point $\boldsymbol{x}$
Require:	Define sample point set $\boldsymbol{X} = \{\boldsymbol{x}^{(i)}, i = 1, 2, ..., N\}$ and corresponding response $y(\boldsymbol{x}^{(i)})$.
Require:	Define the given prediction point $\boldsymbol{x}$.
Require:	Calculate $p_i(\boldsymbol{x})$ in global sample points set $\boldsymbol{X}$.
1.	Define the artificial parameter γ.
2.	Calculate h, $h = \lvert\boldsymbol{x}^{(i)} - \boldsymbol{x}^{(j)}\rvert^2$, the definition of $\boldsymbol{x}^{(i)}$ and $\boldsymbol{x}^{(j)}$ described in Fig. 1.
3.	Initial β, $\beta = \dfrac{\gamma}{h^2}$.
4.	Calculate $\boldsymbol{\lambda^*(x)}$ by a combination of Newton-Raphson algorithm and Nelder-Mead simplex algorithm, $\boldsymbol{\lambda}^*(\boldsymbol{x}) = \arg\min_{\boldsymbol{\lambda}\in\mathbb{R}^n} \log Z(\boldsymbol{x}, \boldsymbol{\lambda})$, $Z(\boldsymbol{x}, \boldsymbol{\lambda}) = \sum_{i=1}^{N} \exp\left[-\beta\lvert\boldsymbol{x} - \boldsymbol{x}^{(i)}\rvert^2 + \boldsymbol{\lambda}\cdot(\boldsymbol{x} - \boldsymbol{x}^{(i)})\right]$.
5.	Calculate $p_i(\boldsymbol{x})$, $p_i(\boldsymbol{x}) = \dfrac{\exp\left[-\beta\lvert\boldsymbol{x} - \boldsymbol{x}^{(i)}\rvert^2 + \boldsymbol{\lambda}^*(\boldsymbol{x})\cdot(\boldsymbol{x} - \boldsymbol{x}^{(i)})\right]}{Z(\boldsymbol{x}, \boldsymbol{\lambda}^*(\boldsymbol{x}))}$.
Require:	Optimization of coefficients $\boldsymbol{C}$.
1.	Define the tolence p_{tol}.
2.	Determin the local neighbourhoods $\boldsymbol{X}_{\text{local}}$ of the prediction point $\boldsymbol{x}$ by selecting $p_i(\boldsymbol{x}) > p_{tol}$.
3.	Calculate $p_i(\boldsymbol{x}^{(i)})$ for each sample point $\boldsymbol{x}^{(i)} \in \boldsymbol{X}_{local}$ based on h, and determin the shape functions matrix $\boldsymbol{p}$.
4.	Calculate coefficients $\boldsymbol{C}$ by $\boldsymbol{C} = \boldsymbol{p}^{-1}\boldsymbol{y}$.
Require:	Calculate $p_i(\boldsymbol{x})$ in local sample points set $\boldsymbol{X}_{local}$.
Require:	Calculate $\hat{y}(\boldsymbol{x})$ for predict point $\boldsymbol{x}$, $\hat{y}(\boldsymbol{x}) = \sum_{i=1}^{M} C_i\, p_i(\boldsymbol{x})$, $\boldsymbol{x}^{(i)} \in \boldsymbol{X}_{local}$.

Nonlinearity of the performance behaviour For convenience, we classify the problems into two categories: low-order nonlinearity (if the square regression $\geq$ 0.85 when using first or second-order polynomial model) and high-order nonlinearity (otherwise).

The test cases are selected from Hock and Schittkowski (1980) which offer 180 problems for testing nonlinear optimization algorithms. While some of the functions exhibit low-order nonlinear behavior, the others are highly nonlinear functions that pose challenges for many surrogate modeling techniques. They are defined as:

(a) A small-scale function with high-order nonlinearity

$$y(\boldsymbol{x}) = 10 + \sum_{i=1}^{n}(x_i^2 + 5\cos(2\pi x_i)), \quad n = 2, -1.0 \leq x_i \leq 1.0. \tag{31}$$

(b) A large-scale function with low-order nonlinearity

$$y(\boldsymbol{x}) = \sum_{i=1}^{n}\left(x_i^2 + x_i \ln\left(\sum_{j=1}^{n} x_j/x_i\right) + \sin(x_i + x_{i+1})\right), \quad n = 5, 0.1 \leq x_i \leq 3.0. \tag{32}$$

(c) A large-scale function with high-order nonlinearity

$$y(\boldsymbol{x}) = \sum_{i=1}^{n}\{(\ln(x_i - 2))^2 + (\ln(10 - x_i))^2\} - \left(\prod_{i=1}^{n}(x_i)^2\right), \quad n = 5, 2.1 \leq x_i \leq 9.9. \tag{33}$$

3.2 Test scheme

3.2.1 Metrics for performance measures

The performances of all surrogate models are measured by the following metrics.

Accuracy The capability of predicting the system response over the design space of interest.

Efficiency In practice, we find that the time difference in constructing different models based on same inputs is not obvious, and it can be neglected when compared with the time needed to complete a sample analysis. So in our research, we mainly consider the number of samples to construct a relatively accurate model as the factor of computation efficiency.

Robustness The capability of achieving good accuracy for different problems. This metric indicates whether a surrogate model is highly problem-dependent.

Convergence When the number of the sample points increases, checking if the accuracy of a surrogate model converges to a stable value.

Transparency The capability of providing the information concerning contributions of different variables and interactions among variables.

For accuracy, the goodness of fit obtained from sample points is not sufficient to assess the accuracy of newly predicted points. Thus, additional error analysis points are employed to verify the accuracy of all the surrogate models, in this paper two different metrics are utilized: R square (R^2) and Normalized Root Mean Squared Error (NRMSE). The definitions of these metrics are given in (34) and (35), respectively.

(a) R square

$$R^2 = 1 - \frac{\sum_{i=1}^{M} \left(y(\boldsymbol{x_i}) - \hat{y}(\boldsymbol{x_i})\right)^2}{\sum_{i=1}^{M} \left(y(\boldsymbol{x_i}) - \bar{y}(\boldsymbol{x_i})\right)^2} = 1 - \frac{\text{MSE}}{variance}, \tag{34}$$

where M is the total number of error analysis points, $\hat{y}(\boldsymbol{x_i})$ is the corresponding predicted value for the observed value $y(\boldsymbol{x_i})$, $\bar{y}(\boldsymbol{x_i})$ is the mean of the observed values. While Mean Square Error (MSE) represents the departure of the surrogate model from the real simulation model, the variance captures how irregular the problem is. The larger the value of R^2, the more accurate the surrogate model.

(b) Normalized Root Mean Squared Error

$$\text{NRMSE} = \frac{\sqrt{\frac{1}{n}\sum_{i=1}^{M}(y(\boldsymbol{x_i}) - \hat{y}(\boldsymbol{x_i}))^2}}{y_{max} - y_{min}} = \frac{\sqrt{\frac{1}{n}\text{MSE}}}{y_{max} - y_{min}}. \tag{35}$$

NRMSE represents the ratio of the MSE to the average of test samples, and it can describe the difference between the predicted points and the actual points. The smaller the NRMSE is, the smaller the error is.

3.2.2 Design of experiments (DOE)

DOE is a strategy for allocating sample points in the design space that aims at maximizing the amount of information acquired. A high-fidelity model (e.g. the exact solution or finite element analysis) is evaluated at these points to create the training data set that is subsequently used to construct the functional surrogate model. When sampling, there is a clear trade-off between the number of points used and the amount of information that can be extracted from these points. The samples are typically spread apart as much as possible in order to capture global trends in the design space.

In this paper, for small-scale test problems, the Full Factorial Experiment (FFE) method (see Koziel et al. 2011) is utilized to create sample points, and for large-scale test problems, the Optimal Latin Hypercube Sampling (OLHS) (see Viana et al. 2010) is employed. The LME-based surrogate model is a type of convex approximation. As a result, the prediction point must be an interior point belonging to the convex hull of its neighboring sample points. To ensure the convergence of the solution of the LME shape functions, in our case study, for the sake of simplicity, the boundary points will be added as sample points to construct the convex hull which ensures any prediction points may be interior points. For a general case, a convex hull algorithm must be employed to check the location of the prediction point relative to its neighboring training points (see Preparata and Franco 1985). The error analysis points will be uniformly distributed on the design space. For a clear demonstration, Fig. 3a and b shows the sampling schemes in the two-dimensional small-scale and large-scale test problems, respectively. In high-dimensional cases, the sampling schemes are similar.

Table 2 lists the experimental designs for test problems. We are interested in examining the performance of all surrogate models when different sample sizes are used for model construction. For each problem, the sample size increases from the least sample point size needed to construct a surrogate model to the sample point size in which the performances of all the surrogate models are stabilized. The construction of PR2, PR4, RBF, KG1 and KG2 surrogate models are performed by using the optimization software ISIGHT, and the construction of the LME-based surrogate model is completed by an in-house program. The performance of all surrogate models is discussed in Section 3.3.

3.3 Performance

3.3.1 Small-scale problems with high-order nonlinearity

As illustrated in Section 2.4, the dimensionless parameter γ is employed to control the locality of the LME shape

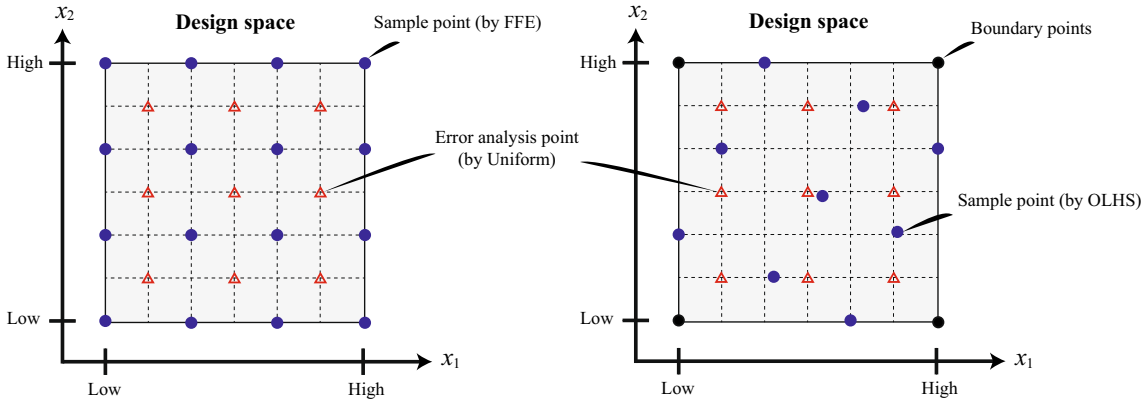

(a) Small-scale problem sampling scheme (b) Large-scale problem sampling scheme

Fig. 3 The hybrid sampling scheme of a two-dimensional case for all test problems

functions. To construct an LME surrogate model, firstly requires defining a γ, which can be readily obtained by comparing several different γ from 0.1 to 6.8 and selected the one with the best approximation performance to build the surrogate model. Table 3 lists the γ values for building LME-based surrogate models of a small-scale problems with high-order nonlinearity (the number of variables $n = 2$) with different sample sizes.

By applying the algorithm in Table 1, the LME-based surrogate models are created with different sample sizes lists in Table 3. The same sample points are utilized to build RBF, PR2, PR4, KG1 and KG2 surrogate models. The performance of all surrogate models is measured by calculating their R^2 and NRMSE metrics as shown in Figs. 4 and 5. As mentioned before, the larger the R square, the more accurate the surrogate model; however, for NRMSE, a smaller value indicates better accuracy. From Fig. 4, it is evident that when the number of sample points is small (25 points), the accuracy of PR2, PR4, RBF, KG1 and KG2 surrogate models is rather poor ($R^2 < 0.3$), while the LME-based surrogate model obtains a good level of accuracy ($R^2 = 0.963563$). As the number of sample points increases, the performance of all models is improved. As shown in Fig. 5, the RBF, KG1 and LME models converge to a high level of fidelity ($R^2 > 0.99, \text{NRMSE} < 0.02$), but the PR2, PR4 and KG2 models reach a fairly low level of fidelity ($R^2 < 0.6, \text{NRMSE} > 0.17$). In addition, the RBF, PR2, PR4 and LME surrogate models exhibit good robustness properties, while KG1 and KG2 are not stable as the number of sample points increases.

3.3.2 Large-scale problems with low-order nonlinearity

Table 4 lists the γ values for building LME-based surrogate models of a large-scale problem with low-order nonlinearity (the number of variables $n = 5$) with different sample sizes. The performance of all surrogate models is measured by calculating their R^2 and NRMSE metrics as shown in Figs. 8 and 9. Figure 6 shows that all surrogate models exhibit good accuracy ($R^2 > 0.8$) by using a small number of sample points (60 points). As the number of sample points increases, the performance of RBF, LME, PR2 and PR4 models become stable and the measurements converge to a high level of fidelity ($R^2 > 0.96, \text{NRMSE} < 0.05$) as shown in Fig. 7, RBF is slightly better than LME, and the accuracies of PR2 and PR4 are very close to each other. On the contrast the KG1 surrogate model experiences severe instabilities with a low level of accuracy (R^2 ranges from 0.45 to 0.8) and the measurements do not converge, which indicates that the KG1 model is not suitable for this type of problems. This circumstance is similar for KG2 surrogate model, but the accuracy and robustness of KG2 are better than KG1.

Table 2 Experimental designs for test problems

Type	Sample points (boundary points included)		Error analysis points		Times
	Method	Size	Method	Size	
Small-scale ($n \leq 3$)	FFE	$(4+i)^n$	Uniform	$(3+i)^n$	$i = 1, 2, \ldots, 8$
Large-scale ($4 \leq n$)	OLHS	$40 + 20i$	Uniform	2^n	

Table 3 Different number of sample points and corresponding γ values for a small-scale problems with high-order nonlinearity

Sample points	25	36	49	64	81	100	121	144
γ	4.8	2.2	0.4	0.4	0.6	0.6	0.6	1.6

3.3.3 Large-scale problems with high-order nonlinearity

The large-scale problem with high-order nonlinearity widely exists in structural reliability analysis, which is one of the most challenging types of problems to be approximated by surrogate models. Table 5 lists the γ values for building LME-based surrogate models of a large-scale problem with high-order nonlinearity (the number of variables $n = 5$) with different sample sizes. The performance of all surrogate models is measured by calculating their R^2 and NRMSE metrics as shown in Figs. 8 and 9. As presented in Fig. 8, when the number of sample points is small (60 points), the accuracy of PR2, PR4 and KG1 surrogate models is low ($R^2 < 0.6$), while the RBF, KG2 and LME-based models show a relatively high level of accuracy ($R^2 = 0.75758$, $R^2 = 0.89243$, $R^2 = 0.838921$, respectively). As the number of sample points increases, the performance of all models is improved. As shown in Fig. 9, the convergence accuracies of KG2 and LME are among the best in the group, their values are very close to each other, and the R^2 and NRMSE metrics of RBF and LME models converge to 1.0 and 0.0 respectively. The accuracy of RBF is also very excellent and takes the third place in the group, but the PR2, PR4 and KG1 models reach a relatively low level of accuracy ($R^2 < 0.83, \text{NRMSE} > 0.11$). Again, the RBF, PR2, PR4 and LME surrogate models exhibit nice robustness properties. For this test case, the KG2 surrogate model reveals a wonderful accuracy and robustness, while KG1 is not stable as the number of sample points less than 180.

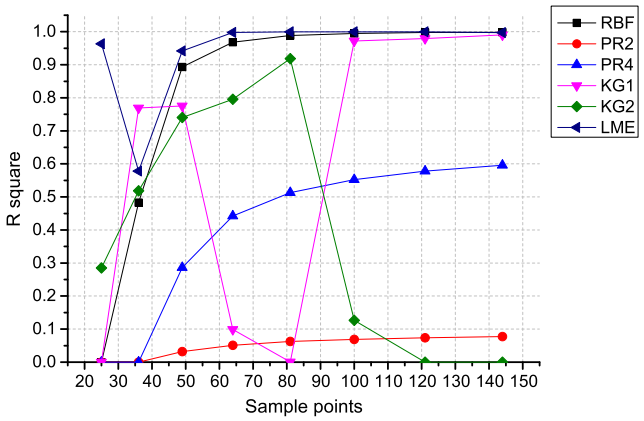

Fig. 4 The relationship between R^2 and the number of sample points for a small-scale problem with high-order nonlinearity

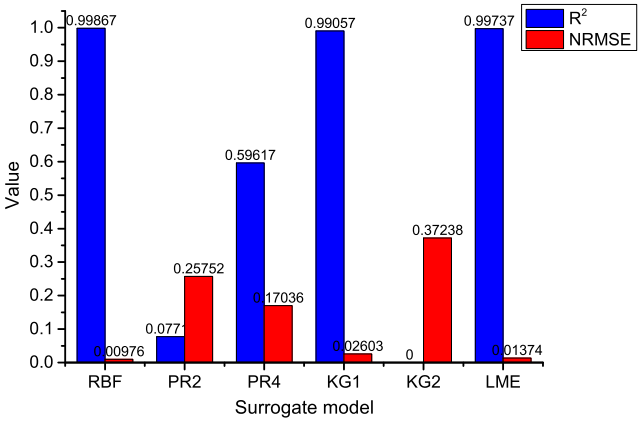

Fig. 5 The statistical data of R^2 and NRMSE of all models for a small-scale problem with high-order nonlinearity (sample point number is 144)

According to the systematic comparative studies presented above, the LME-based surrogate model shows an excellent accuracy and robustness in all the test cases and excels in high order nonlinearity problems with a small number of sample points. As for transparency, PR provides the best transparency in terms of the function relationship and the factor contributions. For RBF, an explicit function exists, however, the factor contributions are not clear. The same holds true for KG. Since the derivatives of LME shape functions are the auxiliary outputs from the calculation and require no extra computational cost as shown in (28), the LME-based surrogate model is of a good transparency.

4 Application

The reliability analysis of aerospace designs is synonymous with the use of time consuming and computationally expensive simulations. This fuels the desire to harness the efficiency of surrogate-based methods in aerospace design reliability analysis. In this section, the proposed LME-based surrogate model will be applied to the turbine disk reliability analysis (TDRA) for Low Cycle Fatigue (LCF) life assessment of a GH720Li turbine disk subjected to geometric uncertainties. For completeness, the TDRA process considering geometric uncertainties is briefly introduced (cf. Fan et al. 2017), which includes four steps (also as outlined in Fig. 10):

Table 4 Different number of sample points and corresponding γ values for a large-scale problem with low-order nonlinearity

Sample points	60	80	100	120	140	160	180	200
γ	4.8	5.8	6.8	6.8	6.8	6.8	6.8	5.8

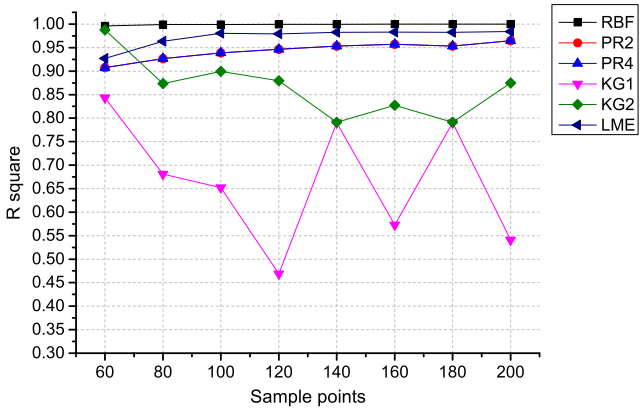

Fig. 6 The relationship between R^2 and the number of sample points for a large-scale problem with low-order nonlinearity

(i) **Selecting key geometric variables.** There is a large number of geometric parameters of a turbine disk, however many of them are non-contribution to the uncertainties of the final design. In TDRA, insignificant geometric variables are screened out by a primary stress sensitivity analysis based on the 1^{st} surrogate model before applying a more informative fatigue life reliability analysis to the remaining set of parameters. As described in Fan et al. (2017), there are 41 geometric parameters of a GH720Li turbine disk (Fig. 11) and an efficient PR surrogate model was constructed by utilizing hundreds of Finite Element stress analysis results. The sensitivity analysis shows that the inner diameter (d_R_1), outer diameter (d_R_2) and rim thickness (d_W_6) contribute most significantly to the variations of the stress distribution in the turbine disk, which are selected as the key variables for the following LCF life analysis.

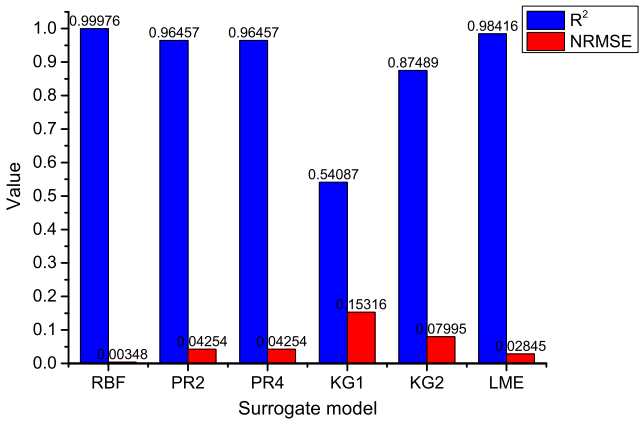

Fig. 7 The statistical data of R^2 and NRMSE of all models for a large-scale problem with low-order nonlinearity (sample point number is 200)

Table 5 Different number of sample points and corresponding γ values for a large-scale problem with high-order nonlinearity

Sample points	60	80	100	120	140	160	180	200
γ	6.8	6.8	3.8	2.2	4.8	4.8	2.8	3.8

(ii) **Determining the probability distributions of the key variables.** For the reliability analysis, the fidelity of the analysis strongly depends on how well we know the underlying distributions of the random variables. In TDRA, the Kolmogorov-Smirnov (K-S) test approach (see Birnbaum 1952; Lilliefors 1967) is adopted to determine the probability distributions of the three key geometric variables.

(iii) **Constructing the 2^{nd} surrogate model.** The 2^{nd} surrogate model is utilized for performing a Monte Carlo Simulation (MCS) of the LCF life of different turbine disk design, which has a small input size but requires extremely high accuracy and efficiency to ensure the credibility of the results. In TDRA, the inputs of the detailed FE simulations are the three key geometric variables and sampled in the design space by OLHS method. These inputs and the resulting LCF life of the turbine disks are used to construct the LME surrogate model.

(iv) **Probability prediction for fatigue life.** The MCS will be performed on the 2^{nd} surrogate model to obtain reliability analysis results.

The material properties of GH720Li at 650 °C and the boundary conditions applied to the disk in the detailed FE simulations of step (iii) are listed in Table 6. All FE simulations are performed in an automated fashion in TDRA and the outputs are the von Mises stress distributions in the tur-

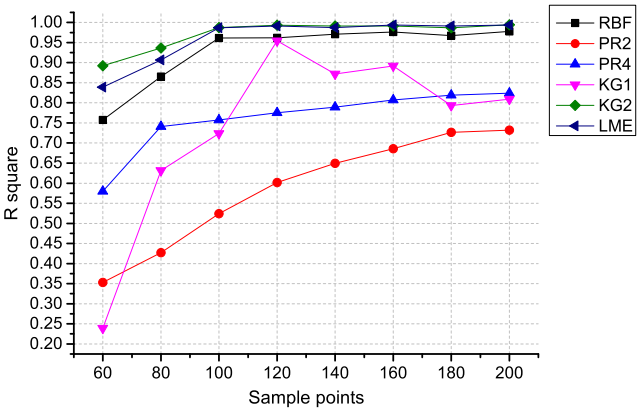

Fig. 8 The relationship between R^2 and the number of sample points for a large-scale problem with high-order nonlinearity

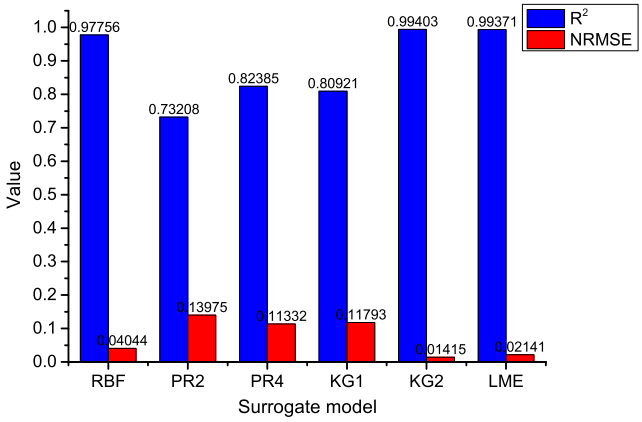

Fig. 9 The statistical data of R^2 and NRMSE of all models for a large-scale problem with high-order nonlinearity (sample point number is 200)

bine disks. The LCF life of the turbine disk is given by the Manson-Coffin model, i.e.,

$$\frac{\Delta\sigma}{2\times 10^{5.2671-0.0003\mu_1}}+10^{0.2102\mu_1}\left(\frac{\Delta\sigma}{2}\times 3.4326\times 10^{-4}\right)^{6.2723}=\left(10^{-\frac{24.1541+3.7741\mu_2}{12.0456+1.7532\mu_2}}-\frac{\sigma_m}{E}\right)\times(2N_f)^{\frac{1}{12.0456+1.7532\mu_2}}+10^{-\frac{2.4733-0.0834\mu_2}{1.9361+0.0494\mu_2}}(2N_f)^{-\frac{1}{1.9361+0.0494\mu_2}}, \tag{36}$$

where, N_f is the LCF life, $\Delta\sigma$ is the stress range, E is the elastic modulus, σ_m is the mean stress, μ_1 and μ_2 are two standard normal random variables, and other constants are obtained from the LCF experiments of GH720Li at 650 °C, more details of the experiments can be found in Fan et al. (2017). In TDRA, the stress range and the mean stress are replaced by the maximum von Mises stress and mean von Mises stress of the turbine disk obtained in FE simulations, respectively. Figure 12 shows the von Mises stress distributions in the turbine disk with different geometric dimensions predicted by FE simulations.

In this work, the number of sample points needed to build the 2^{nd} surrogate model with acceptable accuracy is considered. To this end, the surrogate models using a small scale to a large scale number of sample points are constructed (in this case the size is ranging from 30 to 270). Table 7 lists the sampling scheme for constructing the LME-based surrogate models.

By applying the algorithm in Table 1, the LME-based surrogate models are created according to the FEA results at $30i$ $(i = 1, 2, \ldots, 9)$ number of sample points (Table 8 lists the γ). An example of the FEA results for the case of 270 sample points is illustrated in Fig. 13. In addition, the LCF life of the turbine disks at $4^n (n = 3)$ number of error analysis points predicted by the FE simulations are taken as the physical responses of the system. Thus, the performance of the surrogate models can be assessed by comparing their

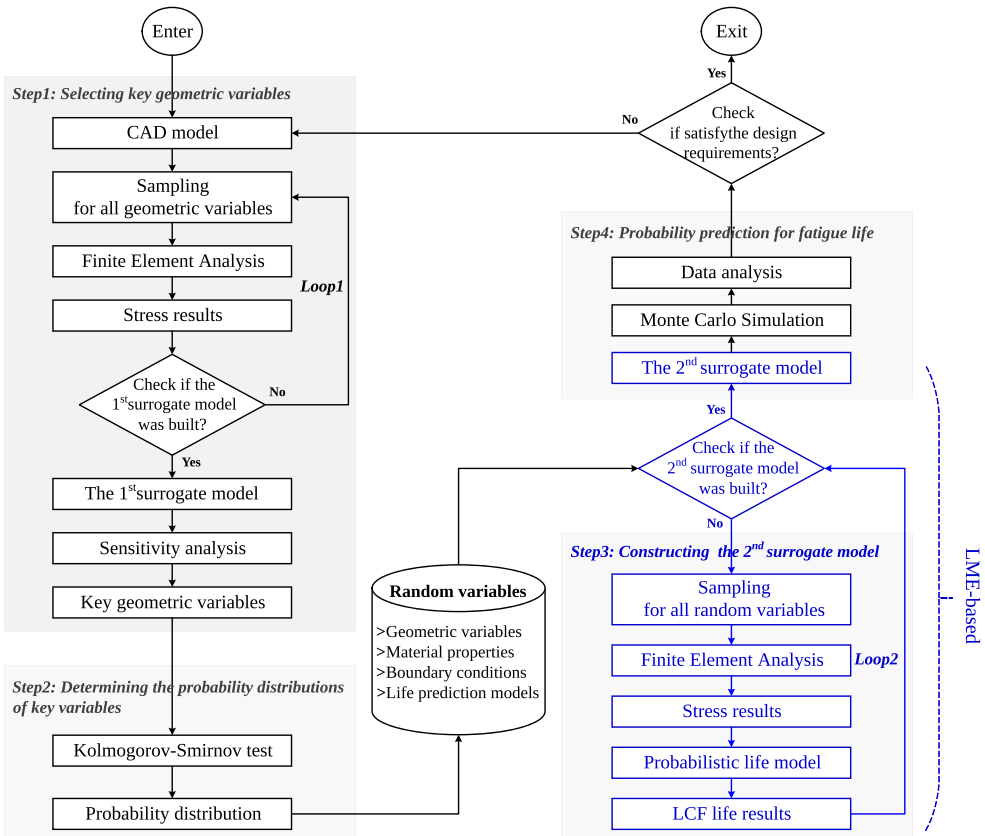

Fig. 10 Flow chart for the reliability analysis of a turbine disk considering geometric uncertainties in TDRA

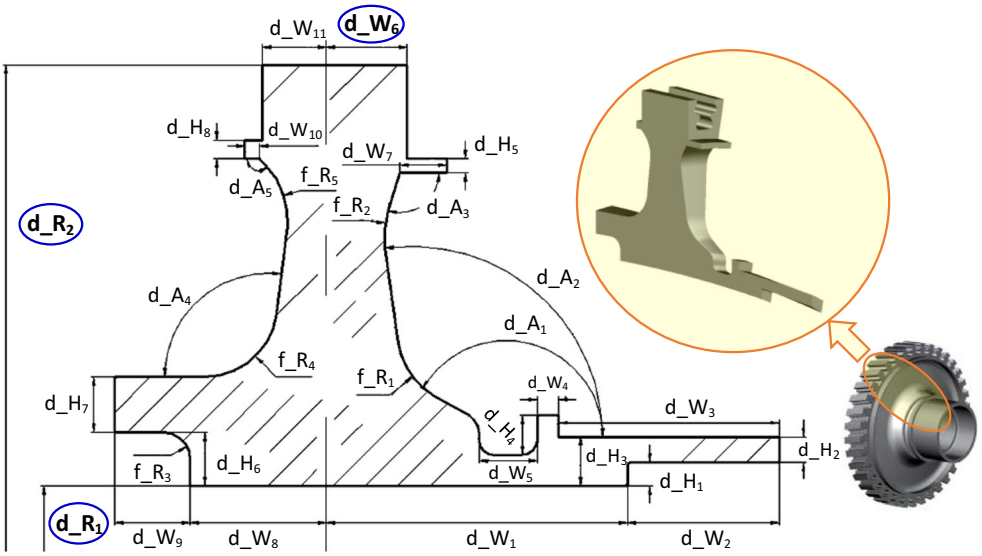

Fig. 11 Variable geometric parameter of the GH720Li turbine disk

approximated LCF life at the error analysis points to the one obtained in FE simulations. Figure 14 shows the relationship between R^2 and the number of sample points for all surrogate models, and Fig. 15 presents the measurements of R^2 and NRMSE for all surrogate models when the number of sample points equals to 270.

As demonstrated in Fig. 14, the performance measurement of all surrogate models converges to a stable value when the number of sample points increases from 30 to 270, among which the LME surrogate model achieves the highest level of accuracy. The R^2 metric of LME-based surrogate model converges to 0.845344 when the number of sample points is greater than 270, and RBF surrogate model obtains a R^2 equal to 0.826016, and KG2 takes the third place in the group ($R^2 = 0.730826$). PR2 and PR4 reach a similar level of accuracy with R^2 equal to 0.674253 and 0.673255, respectively. However, the KG1 surrogate model underperforms noticeably as the number of sample points increases (the accuracy metrics $R^2 = 0$ and NRMSE equal to 1 as shown in Fig. 15), which indicates the KG1 model is not suitable for approximating the LCF life of GH720Li turbine disks. Moreover, it is noted that the performance of PR2 and PR4 models are stable, while the accuracy of LME, RBF and KG2 drops when the number of sample points equals to 180. The PR model is a local approximation scheme, which limits its accuracy in applications to approximate highly nonlinear behaviors with a small scale number of sample points. Under such circumstance, higher-order polynomials can be used, however, instabilities may arise as similar to the RBF and LME-based surrogate models. In addition, it may be difficult to find sufficient sample data to evaluate all of the coefficients in the high-order polynomial equations. KG model is a local approximation scheme, the correlation matrix can become singular if multiple sample points are spaced close to one another or if the sample points are generated from particular designs. On the contrary, the RBF model is a global approximation scheme, in which the shape function covers the whole range of the domain. Approximation of the response function at a given point using RBF surrogate model requires all of the sample data in the design space. Alternatively, the LME-based surrogate model furnishes an effective means of combining the advantages in the local approximation schemes (e.g. PR) and global approximation schemes (e.g. RBF). With the aid of exponential basis functions, the LME-based surrogate model shares similar properties as the RBF model over the problem domain. However, by adjusting γ, the locality of the LME shape functions restricts the contribution of sample points from the local neighborhood.

Three random variables d_R_1, d_R_2 and d_W_6 were considered to obey normal distribution (cf. Fan et al. 2017), and 100,000 sample points were created using Monte-Carlo random sampling method, by conducting 100,000 times MCS on the LME surrogate model, the frequency histogram of LCF life was obtained as shown in Fig. 16a. It can be observed that the LCF life approximately obeys the lognormal distribution within the scope of sampling. The minimum LCF life is 132,092 cycles and the maximum LCF life is 144,286 cycles. When the LCF life equals to 137,492 cycles, it reaches to the highest frequency of 0.05603. In

Table 6 The material properties of GH720Li at 650 °C and the boundary conditions

Name	Density(ρ)	Modulus(E)	Poisson's ratio(ν)	Rotating speed(n)
Value	8140 kg/m^3	2.07E11Pa	0.37	3979.35 rad/s

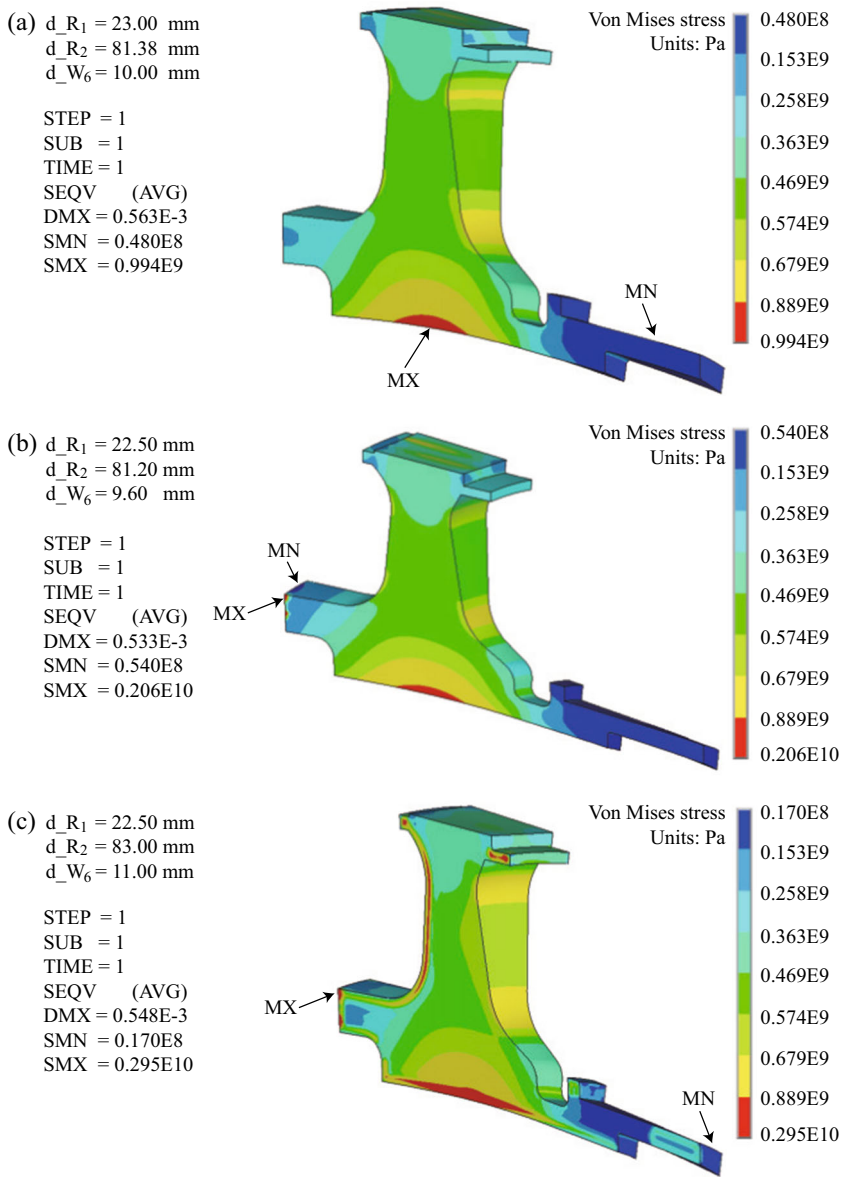

Fig. 12 The von Mises stress distributions in the turbine disk with different geometric dimensions, where d_R_1, d_R_2 and d_W_6 are the three key geometric variables described in Fig. 11 and listed in Table 7

addition, the reliability-life curve was obtained as shown in Fig. 16b. It is evident that although the variation of the dimensional tolerance is small, it still has a significant contribution to the LCF life of turbine disk. Moreover, the LCF life of the GH720Li turbine disk in the reliability of 50, 90, 99 and 99.87% respectively, are listed in Table 9.

Nevertheless, the reliability predicted by the LME surrogate model in Table 9 ignored the modeling error. A simple replacement of the physical response function by a surrogate model does not result in rigorous certification in general, since there is no a priori guarantee that the predictions of the model are of sufficient fidelity. Analysis using surrogate

Table 7 The sampling scheme for 3 random variables

Name	Value(mm)	Sample points(by OLHS) (boundary points included)	Error analysis points (by Uniform)
d_R_1	(22.50, 24.00)	$size = 30i, i = 1, 2, \ldots, 9$	$size = 4^n, n = 3$
d_R_2	(81.20, 83.00)		
d_W_6	(9.60, 11.00)		

Table 8 Different number of sample points and corresponding γ values for building LME-based surrogate models of LCF life

Sample points	30	60	90	120	150	180	210	240	270
γ	0.2	0.2	1.4	0.4	0.2	0.2	2.8	6.8	6.8

models without accounting for their accuracy often underestimates the probability of failure of the system and may lead to undesirable structural design (see Kiureghian and Dakessian 1998; Guo et al. 2009). In order to rigorously quantify the uncertainty of the system by utilizing the surrogate model to replace physical experiments, a model-based Uncertainty Quantification (UQ) methodology is adopted in this work (see Kidane et al. 2012; Adams et al. 2012; Kamga et al. 2014). Specifically, the model-based UQ strategy consists of using the legacy data to establish the level of error of the surrogate model, or modeling error, and to subsequently use the validated model as a basis for the determination of probabilities of outcomes. The quantification of modeling uncertainty establishes, to a specified confidence, the probability that the actual response of the system lies within a certain distance of the model. Once the extent of model uncertainty has been established in this manner, the LME surrogate model can be conveniently used to stand in for the actual or empirical response of the system with a factor of confidence. In this example, the LCF life of GH720Li turbine disks can be modeled by the response function $Y = G(\boldsymbol{X})$, which maps the random geometric parameters, $\boldsymbol{X} = (d\_R_1, d\_R_2, d\_W_6) \in S$ where S is the feasible set of input parameters, to the LCF life Y. Thus, certification of the LCF life assessment requires $P[G(\boldsymbol{X}) \leq a] \leq \epsilon$, i.e., the probability of the LCF life of turbine

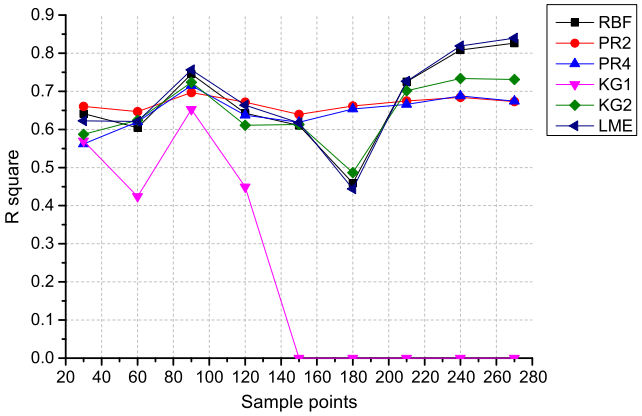

Fig. 14 The relationship between R^2 and the number of sample points for approximating the LCF life of the GH720Li turbine disk

disks less than a user-specified design criterion a should be smaller than some appropriate certification tolerance ϵ. This condition expresses the requirement that the probability of failure (PoF) of the system be acceptably small. In the model-based UQ framework, the PoF is bounded by using the McDiarmid's inequality and Martingale theory as

$$P[G(\boldsymbol{X}) \leq a] \leq \exp\left(-2\frac{(E_m[G] - a - \alpha)_+^2}{D_G^2}\right), \tag{37}$$

where $E_m[G]$ and α are the empirical mean of the LCF life predicted by FEA and a margin hit that compensates for the use of an empirical mean, respectively (see McDiarmid 1989, 1997; Lucas et al. 2008; Habib et al. 2013). The spread of the response function, also known as *system*

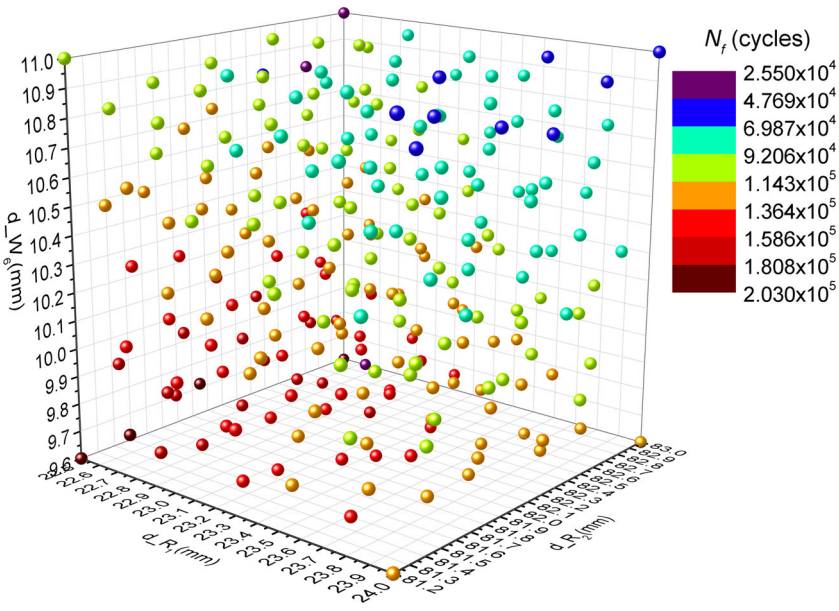

Fig. 13 An example of the FEA results for the case of 270 sample points, where d_R_1, d_R_2 and d_W_6 are the three key geometric variables listed in Table 7, and N_f is the LCF life as described in (36)

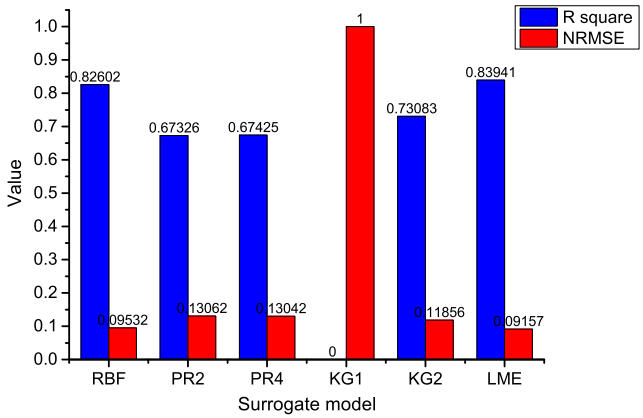

Fig. 15 The statistical data of R^2 and NRMSE of all models for approximating the LCF life of the GH720Li turbine disk (sample point number is 270)

uncertainty or *system diameter*, is denoted as D_G, which can be calculated by

$$D_G = \sup\|G(\boldsymbol{X}^{(i)}) - G(\boldsymbol{X}^{(j)})\| \quad \text{for} \forall \boldsymbol{X}^{(i)}, \boldsymbol{X}^{(j)} \in S. \tag{38}$$

In our implementation, we performed $m = 334$ tests at sample points and error analysis points (270 sample points and 64 error analysis points). Thus, the empirical mean $E_m[G]$ and margin hit α may be obtained as,

$$E_m[G] = \frac{1}{m}\sum_{i=1}^{m} Y_i, \tag{39}$$

and,

$$\alpha = \frac{D_G}{\sqrt{m}}(-\log\epsilon')^{1/2}, \tag{40}$$

Table 9 The typical life-reliability results

Reliability	50%	90%	99%	99.87%
LCF life	134983 cycles	134014 cycles	133036 cycles	132225 cycles

where $\epsilon' = 0.01$ is a prespecified estimation tolerance. According to the definition of the system uncertainty, quantification of D_G entails the solution of three global optimization problems for the evaluation of sub-diameters for each of the input parameters $\{d\_R_1, d\_R_2, d\_W_6\}$. Since global optimization algorithms typically converge slowly, the evaluation of uncertainties directly from laboratory testing may be prohibitively expensive and time consuming. One of the key component of the model-based UQ methodology is to determine the upper bound of D_G following from the triangular-inequality,

$$D_G = D_{G-F+F} \leq D_{(G-F)} + D_F, \tag{41}$$

where $F(\boldsymbol{X})$ is the LCF life predicted by LME-based surrogate model. D_F is defined as the *model uncertainties*, i.e., the biggest deviation in the LCF life predicted by the LME-based surrogate model which can be calculated directly from the probability distribution shown in Fig. 16. The requisite quantitative measure of model fidelity is supplied by the *modeling error*, $D_{G-F} = \sup\|G(\boldsymbol{X}^{(i)}) - F(\boldsymbol{X}^{(i)}) - G(\boldsymbol{X}^{(j)}) + F(\boldsymbol{X}^{(j)})\|$ for $\forall \boldsymbol{X}^{(i)}, \boldsymbol{X}^{(j)} \in S$. Finally, the probability of failure of the TDRA process is bounded by the McDiarmid's inequality,

$$P[G(\boldsymbol{X}) \leq a] \leq \exp\left(-2\frac{M^2}{U^2}\right), \tag{42}$$

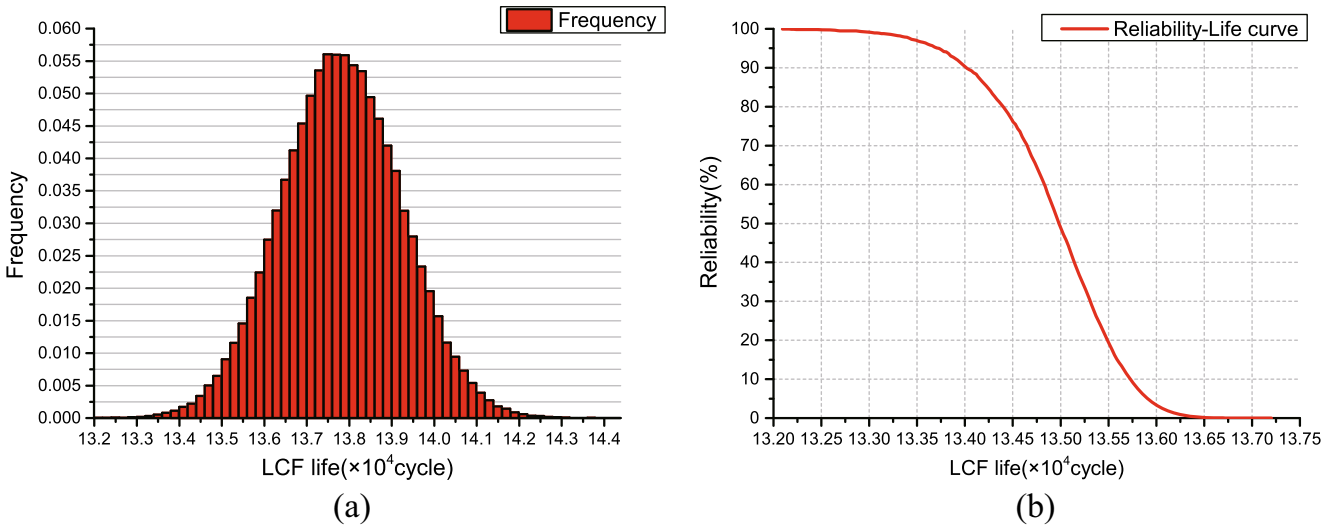

Fig. 16 **a** The frequency histogram of the LCF life, **b** the reliability-life curve of the GH720Li turbine disk

Table 10 Summary of results from the UQ analysis of the TDRA for LCF life assessment

Empirical mean LCF life ($E_m[G]$) :	150544 cycles
Margin hit (α for $\epsilon' = 0.01$) :	1010 cycles
Model uncertainties (D_F) :	12194 cycles
Modeling error (D_{G-F}) :	4640 cycles
Total uncertainty ($U = D_{G-F} + D_F$) :	16834 cycles

Threshold a	Total margin $M = E_m[G] - a - \alpha$	Confidence factor M/U
134983 cycles	14551 cycles	0.864405
134014 cycles	15520 cycles	0.921967
133036 cycles	16498 cycles	0.980064
132225 cycles	17309 cycles	1.028240

where M is the *design margin* and describes the difference between the mean performance and the design criterion,

$$M = [E_m[G] - a - \alpha]_+, \tag{43}$$

and U represents the *system uncertainty*,

$$U = D_{G-F} + D_F, \tag{44}$$

finally, the confidence factor (CF) is given by,

$$CF = \frac{M}{U}. \tag{45}$$

If CF is larger than 1.0, the TDRA process considering geometric uncertainties may be regarded as efficient and a candidate for certification. Summary of results from the UQ analysis of the TDRA for LCF life assessment of GH720Li turbine disks subjected to geometric uncertainties are listed in Table 10.

5 Conclusions

In this paper, a new approach for constructing surrogate models from sample data based on the local Maximum Entropy (LME) approximation scheme is proposed. The performance of the LME-based surrogate model is systematically investigated by comparing to the conventional surrogate models (PR, RBF and KG) in three types of test problems. The robustness and efficiency of the LME-based surrogate model is further demonstrated in the application of the turbine disk reliability analysis. Finally, a model-based UQ analysis, that identifies the error of the LME-based surrogate model, is performed to rigorously quantify the uncertainty of the system. In our studies, the LME-based surrogate model shows an excellent level of accuracy and robustness in all test cases as well as in the engineering problem, and excels in high order nonlinearity problems with a small number of sample points. This attractive property is derived from the calculation of the LME shape functions, which requires fewer sampling points and can be carried out robustly and efficiently in any spatial dimensions. In addition, the derivatives of the LME shape functions are auxiliary outputs of the computation without any additional computational cost, which increases the transparency of the model. It's worth noting that the LME shape functions are allowed to depend on the location of the prediction point and have the potential to adjust themselves adaptively by varying γ in order to achieve optimal degrees of locality. Nevertheless, the focus of this work is to introduce a new method for the construction of surrogate models based on the LME approximation scheme. Therefore, the values of γ are selected manually in our numerical experiments to adjust the locality of the shape functions. Future ongoing work is to develop a self-adaptive LME-based surrogate model by taking the advantage of the adaptive property of LME shape functions, which may enable a great reduction of the number of sample points necessary for constructing a surrogate model while maintaining a high level of accuracy. Overall, the LME-based surrogate model enables a seamless bridge between local and global approximation schemes.

Acknowledgements This work is supported by the State Scholarship Fund of China (File No.201506020025), National Natural Science Foundation of China (File No.51275024) and Aviation Science Foundation of China (File No.2014ZB51). The authors are grateful for these supports.

References

Adams M, Lashgari A, Li B, McKerns M, Mihaly J, Ortiz M, Owhadi H, Rosakis A, Stalzer M, Sullivan T (2012) Rigorous model-based uncertainty quantification with application to terminal ballistics—part ii. systems with uncontrollable inputs and large scatter. J Mech Phys Solids 60(5):1002–1019

Arroyo M, Ortiz M (2006) Local maximum-entropy approximation schemes: a seamless bridge between finite elements and meshfree methods. Int J Numer Methods Eng 65(13):2167–2202

Barton RR (1992) Metamodels for simulation input-output relations. In: Proceedings of the 24th conference on Winter simulation. ACM, pp 289–299

Birnbaum ZW (1952) Numerical tabulation of the distribution of Kolmogorov's statistic for finite sample size. J Am Stat Assoc 47(259):425–441

Bucher CG, Bourgund U (1990) A fast and efficient response surface approach for structural reliability problems. Struct Saf 7(1):57–66
Das PK, Zheng Y (2000) Cumulative formation of response surface and its use in reliability analysis. Probab Eng Mech 15(4):309–315
Deng J (2006) Structural reliability analysis for implicit performance function using radial basis function network. Int J Solids Struct 43(11–12):3255–3291. doi:10.1016/j.ijsolstr.2005.05.055
Echard B, Gayton N, Lemaire M (2011) AK-MCS: an active learning reliability method combining Kriging and Monte Carlo Simulation. Struct Saf 33(2):145–154. doi:10.1016/j.strusafe.2011.01.002
Elhewy AH, Mesbahi E, Pu Y (2006) Reliability analysis of structures using neural network method. Probab Eng Mech 21(1):44–53
Fan J, Liao H, Li D, Wang R, Hu D (2017) Probabilistic analysis of turbine disk fatigue life considering geometric uncertainties. J Aerosp Pow 32(1):66–74
Forrester AIJ, Keane AJ (2009) Recent advances in surrogate-based optimization. Prog Aerosp Sci 45(1–3):50–79. doi:10.1016/j.paerosci.2008.11.001
Fraternali F, Lorenz CD, Marcelli G (2012) On the estimation of the curvatures and bending rigidity of membrane networks via a local maximum-entropy approach. J Comput Phys 231(2):528–540. doi:10.1016/j.jcp.2011.09.017
Golub GH, Van Loan CF (2012) Matrix computations, vol 3. JHU Press
González D, Cueto E, Doblaré M (2010) A higher order method based on local maximum entropy approximation. Int J Numer Methods Eng 83(6):741–764. doi:10.1002/nme.2855
Guan XL, Melchers RE (2001) Effect of response surface parameter variation on structural reliability estimates. Struct Saf 23(4):429–444
Guo Z, Bai G (2009) Application of least squares support vector machine for regression to reliability analysis. Chin J Aeronaut 22(2):160–166
Guo X, Bai W, Zhang W, Gao X (2009) Confidence structural robust design and optimization under stiffness and load uncertainties. Comput Methods Appl Mech Eng 198(41):3378–3399. doi:10.1016/j.cma.2009.06.018
Habib M, McDiarmid C, Ramirez-Alfonsin J, Reed B (2013) Probabilistic methods for algorithmic discrete mathematics, vol 16. Springer Science & Business Media
Hock W, Schittkowski K (1980) Test examples for nonlinear programming codes. J Optim Theory Appl 30(1):127–129
Hurtado JE, Alvarez DA (2001) Neural-network-based reliability analysis: a comparative study. Comput Methods Appl Mech Eng 191(1):113–132
Jin R, Chen W, Simpson TW (2001) Comparative studies of metamodelling techniques under multiple modelling criteria. Struct Multidiscip Optim 23(1):1–13
Journel AG, Huijbregts CJ (1978) Mining geostatistics. Academic Press
Kamga PH, Li B, McKerns M, Nguyen L, Ortiz M, Owhadi H, Sullivan T (2014) Optimal uncertainty quantification with model uncertainty and legacy data. J Mech Phys Solids 72:1–19. doi:10.1016/j.jmps.2014.07.007
Kaymaz I, McMahon CA (2005) A response surface method based on weighted regression for structural reliability analysis. Probab Eng Mech 20(1):11–17
Kidane A, Lashgari A, Li B, McKerns M, Ortiz M, Owhadi H, Ravichandran G, Stalzer M, Sullivan TJ (2012) Rigorous model-based uncertainty quantification with application to terminal ballistics, part i: Systems with controllable inputs and small scatter 60(5):983–1001. doi:10.1016/j.jmps.2011.12.001
Kim SH, Na SW (1997) Response surface method using vector projected sampling points. Struct Saf 19(1):3–19
Kiureghian AD, Dakessian T (1998) Multiple design points in first and second-order reliability. Struct Saf 20(1):37–49. doi:10.1016/S0167-4730(97)00026-X
Kochmann DM, Venturini GN (2014) A meshless quasicontinuum method based on local maximum-entropy interpolation. Model Simul Mater Sci Eng 22(3) 034:007. doi:10.1088/0965-0393/22/3/034007
Koziel S, Ciaurri DE, Leifsson L (2011) Surrogate-based methods. In: Koziel S, Yang XS (eds) Computational optimization, methods and algorithms, no. 356 in studies in computational intelligence. Springer Berlin Heidelberg, pp 33–59. doi:10.1007/978-3-642-20859-1_3
Li B, Habbal F, Ortiz M (2010) Optimal transportation meshfree approximation schemes for fluid and plastic flows. Int J Numer Methods Eng 83(12):1541–1579
Li J, Wang H, Kim NH (2012) Doubly weighted moving least squares and its application to structural reliability analysis. Struct Multidiscip Optim 46(1):69–82
Lilliefors HW (1967) On the Kolmogorov-Smirnov test for normality with mean and variance unknown. J Am Stat Assoc 62(318):399–402
Liu YW, Moses F (1994) A sequential response surface method and its application in the reliability analysis of aircraft structural systems. Struct Saf 16(1-2):39–46
Lucas LJ, Owhadi H, Ortiz M (2008) Rigorous verification, validation, uncertainty quantification and certification through concentration-of-measure inequalities. Comput Methods Appl Mech Eng 197(51):4591–4609
McDiarmid C (1989) On the method of bounded differences. Surv Combinatorics 141(1):148–188
McDiarmid C (1997) Centering sequences with bounded differences. Comb Probab Comput 6(01):79–86
Most T (2007) An adaptive response surface approach for structural reliability analyses based on support vector machines. In: Proceedings of the eleventh international conference on civil, structural and environmental engineering computing, BHV Topping
Nelder JA, Mead R (1965) A simplex method for function minimization. Comput J 7(4):308–313
Nguyen XS, Sellier A, Duprat F, Pons G (2009) Adaptive response surface method based on a double weighted regression technique. Probab Eng Mech 24(2):135–143
Ortiz A, Puso MA, Sukumar N (2010) Maximum-entropy meshfree method for compressible and near-incompressible elasticity. Comput Methods Appl Mech Eng 199(25–28):1859–1871. doi:10.1016/j.cma.2010.02.013
Panda SS, Manohar CS (2008) Applications of meta-models in finite element based reliability analysis of engineering structures. Comput Model Eng Sci 28:161–184
Papadrakakis M, Papadopoulos V, Lagaros ND (1996) Structural reliability analyis of elastic-plastic structures using neural networks and Monte Carlo simulation. Comput Methods Appl Mech Eng 136(1):145–163
Preparata SM, Franco P (1985) Computational geometry - an introduction | Franco P. Preparata | Springer
Queipo NV, Haftka RT, Shyy W, Goel T, Vaidyanathan R, Kevin Tucker P (2005) Surrogate-based analysis and optimization. Prog Aerosp Sci 41(1):1–28. doi:10.1016/j.paerosci.2005.02.001
Rajashekhar MR, Ellingwood BR (1993) A new look at the response surface approach for reliability analysis. Struct Saf 12(3):205–220
Rosolen A, Arroyo M (2013) Blending isogeometric analysis and local maximum entropy meshfree approximants. Comput Methods Appl Mech Eng 264:95–107. doi:10.1016/j.cma.2013.05.015
Simpson TW, Lin DK, Chen W (2001) Sampling strategies for computer experiments: design and analysis. Int J Reliability Appl 2(3):209–240
Song CY, Lee J, Mo Choung J (2011) Reliability-based design optimization of an FPSO riser support using moving least squares response surface meta-models. Ocean Eng 38(2–3):304–318. doi:10.1016/j.oceaneng.2010.11.001

Song H, Choi KK, Lee I, Zhao L, Lamb D (2013) Adaptive virtual support vector machine for reliability analysis of high-dimensional problems. Struct Multidiscip Optim 47(4):479–491

Ullah Z, Coombs WM, Augarde CE (2013) An adaptive finite element/meshless coupled method based on local maximum entropy shape functions for linear and nonlinear problems. Comput Methods Appl Mech Eng 267:111–132. doi:10.1016/j.cma.2013.07.018

Viana FA, Venter G, Balabanov V (2010) An algorithm for fast optimal Latin hypercube design of experiments. Int J Numer Methods Eng 82(2):135–156

Wild S, Regis R, Shoemaker C (2008) ORBIT: optimization by radial basis function interpolation in trust-regions. SIAM J Sci Comput 30(6):3197–3219. doi:10.1137/070691814

Wong FS (1985) Slope reliability and response surface method. J Geotech Eng 111(1):32–53

Wu CT, Young DL, Hong HK (2013) Adaptive meshless local maximum-entropy finite element method for convection–diffusion problems. Comput Mech 53(1):189–200. doi:10.1007/s00466-013-0901-4

Youn BD, Choi KK (2004) A new response surface methodology for reliability-based design optimization. Commun Strateg 82(2–3):241–256. doi:10.1016/j.compstruc.2003.09.002

Zhao L, Choi KK, Lee I (2011) Metamodeling method using dynamic kriging for design optimization. AIAA J 49(9):2034–2046

Zhao L, Choi KK, Lee I, Gorsich D (2013) Conservative surrogate model using weighted kriging variance for sampling-based RBDO. J Mech Des 091(9):003